Inorganic Chemistry
including bioinorganic chemistry

Article

Star-Shaped Molecule of MnO Core with an *S* = 10 High-Spin State. A Theoretical and Experimental Study with XPS, XMCD, and Other Magnetic Methods

Sumit Khanra, Karsten Kuepper, Thomas Weyhermu#ller, Manuel Prinz, Michael Raekers, Sebastian Voget, Andrei V. Postnikov, Frank M. F. de Groot, Simon J. George, Marin Coldea, Manfred Neumann, and Phalguni Chaudhuri

Inorg. Chem., **2008**, 47 (11), 4605-4617 • DOI: 10.1021/ic7023007 • Publication Date (Web): 06 May 2008

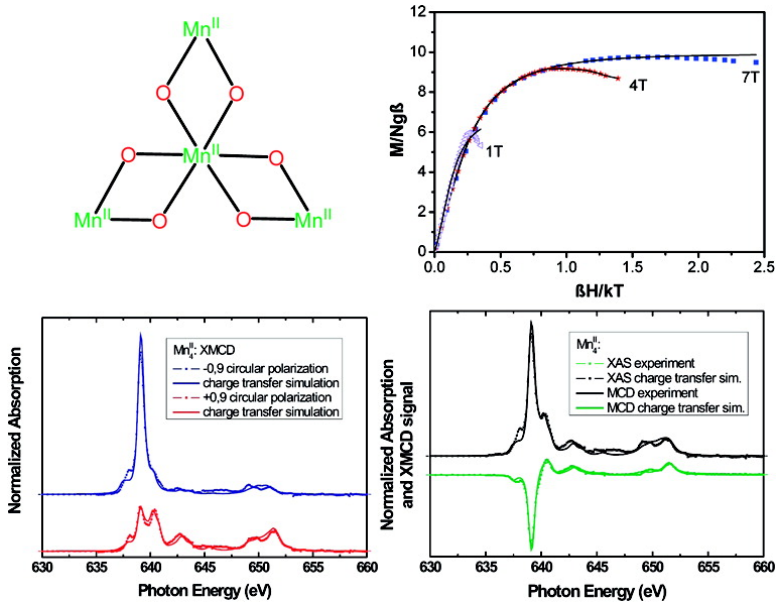

More About This Article

Additional resources and features associated with this article are available within the HTML version:

- Supporting Information
- Links to the 1 articles that cite this article, as of the time of this article download
- Access to high resolution figures
- Links to articles and content related to this article
- Copyright permission to reproduce figures and/or text from this article

Inorg. Chem. **2008**, *47*, 4605−4617

Inorganic Chemistry
Article

Star-Shaped Molecule of $Mn^{II}_4O_6$ Core with an $S_t = 10$ High-Spin State. A Theoretical and Experimental Study with XPS, XMCD, and Other Magnetic Methods

Sumit Khanra,[†] Karsten Kuepper,[‡] Thomas Weyhermüller,[†] Manuel Prinz,[§] Michael Raekers,[§] Sebastian Voget,[§] Andrei V. Postnikov,[||] Frank M. F. de Groot,[⊥] Simon J. George,[#] Marin Coldea,[▽] Manfred Neumann,[*,§] and Phalguni Chaudhuri[*,†]

Max-Planck-Institut für Bioanorganische Chemie, Stiftstrasse 34−36, D-45470 Mülheim an der Ruhr, Germany, Forschungszentrum Dresden-Rossendorf, Institute of Ion Beam Physics and Materials Research, P.O. Box 510119, D-01314 Dresden, Germany, Department of Physics, University of Osnabrück, Barbarastrasse 7, D-49069 Osnabrück, Germany, Laboratoire de Physique des Milieux Denses, Institute de Physique Electronique et Chimie, Paul Verlaine University, 1 Bd Arago, F-57078 Metz, France, Department of Inorganic Chemistry and Catalysis, Utrecht University, Sorbonnelaan 16, 3584 CA Utrecht, The Netherlands, Advanced Biological and Environmental X-ray Facility, Lawrence Berkeley National Laboratory, 1 Cyclotron Road, Berkeley, California 94720, and Faculty of Physics, University Babes—Bolyai, R-3400 Cluj—Napoca, Romania

Received November 22, 2007

We report a comprehensive study of the electronic and magnetic properties of a star-shaped molecule comprising a $Mn^{II}_4O_6$ core. One feature of this compound is weak magnetic coupling constants compared to other similar polyoxo compounds. This leads to complicated low-lying magnetic states in which the ground state is not well separated from the upper-lying states, yielding a high-spin molecule with a giant magnetic moment of up to 20 μ_B/formula unit. We apply X-ray diffraction and magnetometry as well as other X-ray spectroscopic techniques, namely, X-ray photoelectron spectroscopy, X-ray magnetic circular dichroism, and X-ray emission spectroscopy. We compare our experimental results with ab initio electronic band structure calculations as well as the localized electronic structure around the Mn^{2+} ions with charge-transfer multiplet calculations.

1. Introduction

Exchange-coupled polymetallic complexes, in which spin coupling between paramagnetic metal ions is propagated via bridging atoms, are of special interest to researchers who seek new molecule-based magnetic materials[1,2] displaying interesting electronic properties and to bioinorganic chemists who investigate the structure and function of polynuclear metal centers in proteins.[3]There is an impressive diversity of spin-coupled structures in biology, e.g., ascorbate oxidase, cytochrome oxidase, ribonucleotide reductase, water-oxidizing complex of photosystem II, etc. The intimate relationship between spin coupling and molecular structure has fostered, on the other hand, the emergence of molecular magnetism as a multidisciplinary field.[4]The fundamental understanding regarding the factors that determine the spin states of polynuclear transition-metal complexes owes much to the study of model compounds where magnetostructural correlations can be established in a systematic way. To achieve this goal, the influence of parameters such as the symmetry of magnetic orbitals,

* To whom correspondence should be addressed. E-mail: mneumann@uos.de (M.N.), chaudh@mpi-muelheim.mpg.de (P.C.).
[†] Max-Planck-Institut für Bioanorganische Chemie.
[‡] Institute of Ion Beam Physics and Materials Research.
[§] University of Osnabrück.
[||] Paul Verlaine University.
[⊥] Utrecht University.
[#] Lawrence Berkeley National Laboratory.
[▽] University Babes—Bolyai.

(1) (a) *Magnetic Molecular Materials*; Gatteschi, D., Kahn, O., Miller, J. S., Palacio, F., Eds.; Kluwer Academic Publishers: Dordrecht, The Netherlands, 1991. (b) *Research Frontiers in Magnetochemistry*; O'Connor, C. J., Ed.; World Scientific: Singapore, 1993. (c) A tribute to Oliver Kahn: *J. Solid State Chem.* **2001**, *159* No. 2 (July). (d) *Magnetism: Molecules to Materials*; Miller, J. S., Brillon, M., Eds.; Wiley-VCH: Weinheim, Germany, 2002.

10.1021/ic7023007 CCC: $40.75
Published on Web 05/06/2008

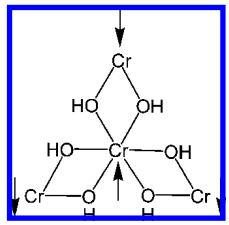

Figure 1. Chromium(III) analogue of Werner's hexol.

the nature of bridging and terminal ligands, and changes in coordination geometry is being studied. Surprisingly, few studies of the influence of the molecular topology on the magnetic properties of coordination complexes have been performed.[5] For example, the chromium(III) analogue of the Werner's hexol, $[Cr^{III}\{(OH)_2Cr^{III}en_2\}_3](ClO_4)_6$ exhibits a high-spin $S_t = 3$ ground state[6] owing to its topology, as shown in Figure 1.

A ferromagnetic-like behavior is obtained with a ground state characterized by a large spin, although the interaction between the nearest-neighbor Cr^{III} ions ($S_{Cr} = {}^3/_2$) is antiferromagnetic. This effective ferromagnetic coupling between the outer ions is very interesting in the context of synthesizing "high-spin" molecules. The best result would be obtained in a topology where a maximum number of spins align in the same direction, as shown in Figure 1. The other two topological possibilities for tetranuclear complexes, namely, the square and the linear arrangements, led in the case of identical metal ions to a diamagnetic ground state because of the equal number of spins in each direction. Thus, it is possible to tune the magnetic properties of polynuclear complexes by controlling the topology and the nature of the ions in the interaction. This approach is particularly promising for the synthesis of "high-spin" molecules. Of particular concern in this context is the development of synthetic routes that can provide high nuclear metal complexes with high spins in a controlled fashion. Among the variety of methodologies applied to synthesize polymetallic coordination compounds, the use of "metalloligands", i.e., metal complexes as ligands,[7] in which the ligands already bound to one metal have a free lone pair of electrons for coordination to a second metal of the same or different kind, has proven to be very successful; this route offers many potential advantages over the self-assembled route in which no control upon the products that are formed is possible, whereas the approach of using metalloligands proceeds step by step and

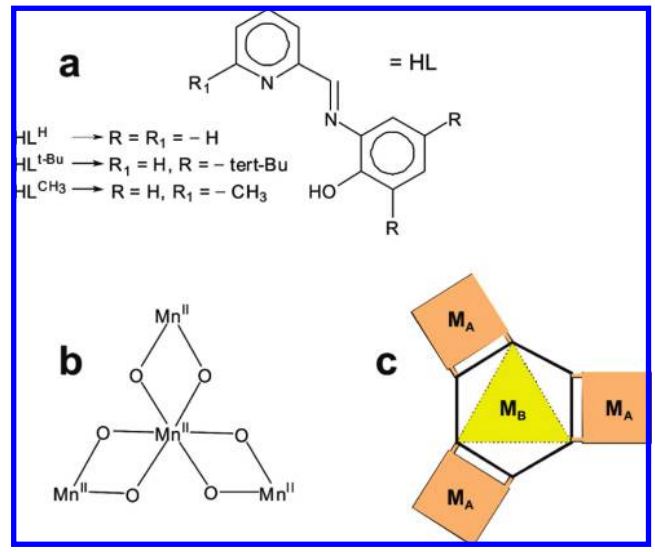

Figure 2. (a) Formula and abbreviations of the ligands used. (b) Core structure of compound **2** illustrating the topology of the high-spin d^5 Mn^{II} ions. (c) Concept of "metal complexes as ligands" depicted in modular form.

provides a route to gaining control of the nuclearity in addition to the preparation of species containing different metal ions, i.e., heterometallic complexes. We have been favoring the strategy of using "complexes as ligands" for a few years and have already reported star-shaped tetranuclear molecules like $Ni^{II}(Ni^{II}L)_3$[8] and $Cr^{III}(Mn^{II}\text{-oxime})_3$,[9] as depicted in the modular form (Figure 2). As a continuation of our interest in phenol-containing ligands,[10] we report here the use of a mononuclear, neutral manganese(II) complex $Mn^{II}L_2$ (**1**), in which the phenoxo oxygen atoms of the tridentate ligand $[L]^-$ occupy the cis position, as a building block to generate the star-shaped Mn_4O_6 motif (Figure 2).

In this paper, we explore the electronic and magnetic properties of the star-shaped molecule of the Mn_4O_6 core. Similar to the iron star molecule,[11,12] it is expected that the spins of the outer three manganese ions will couple antiparallel to that of the central ion, leading to an overall

(2) Kahn, O. *Molecular Magnetism*; VCH: New York, 1993.
(3) (a); Holm, R. H.; Solomon, E. I., Guest Eds. *Chem. Rev.* **1996**, *96* (7); **2004**, *104* (2). (b) *Bioinorganic Chemistry of Copper*; Karlin, K. D., Tyeklár, Z., Eds.; Chapman & Hall: New York, 1993. (c) *Mechanistic Bioinorganic Chemistry*; Holden, H. T., Pecoraro, V. L., Eds.; American Chemical Society: Washington, DC, 1995. (d) *Handbook of Metalloproteins*; Messerschmidt A., Huber, R., Poulos, T., Wieghardt, K., Eds.; John Wiley & Sons: Chichester, U.K., 2001.
(4) (a) Christou, G.; Gatteschi, D.; Hendnrickson, D. N.; Sessoli, R. *MRS Bull.* **2000**, *25*, 66. (b) Gatteschi, D.; Sessoli, R. *Angew. Chem., Int. Ed.* **2003**, *42*, 268. (c) Bircher, R.; Chaboussard, G.; Dobe, C.; Güdel, H. U.; Ochsenbein, S. T.; Sieber, A.; Waldmann, O. *Adv. Funct. Mater.* **2006**, *16*, 209.
(5) (a) Lloret, F.; Journaux, Y.; Julve, M. *Inorg. Chem.* **1990**, *29*, 3967. (b) Hodgson, D. J.; Michelsen, K.; Pedersen, E.; Towle, D. K. *Inorg. Chem.* **1991**, *30*, 815.
(6) (a) Andersen, P.; Berg, T. *Acta Chem. Scand., Ser. A* **1978**, *32*, 989. (b) Güdel, H.; Hauser, U. *Inorg. Chem.* **1980**, *19*, 1325.
(7) (a) Kahn, O. *Adv. Inorg. Chem.* **1995**, *43*, 179. (b) Gruber, S. J.; Harris, C. M.; Sinn, E. *J. Inorg. Nucl. Chem.* **1968**, *30*, 1805. (c) Selbin, J.; Ganguly, L. *J. Inorg. Nucl. Chem. Lett.* **1969**, *5*, 715. (d) Singh, C. B.; Sahoo, B. *J. Inorg. Nucl. Chem.* **1974**, *36*, 1259. (e) Linkvedt, R. L.; Kramer, L. S.; Ranger, G.; Corfield, P. W.; Glick, M. D. *Inorg. Chem.* **1983**, *22*, 3580. (f) Luneau, D.; Oshio, H.; Okawa, H.; Kida, S. *J. Chem. Soc., Dalton Trans.* **1990**, 2283. (g) Chaudhuri, P.; Winter, M.; Fleischhauer, P.; Haase, W.; Flörke, U.; Haupt, H.-J. *J. Chem. Soc., Chem. Commun.* **1990**, 1728.
(8) Pavlishchuk, V.; Birkelbach, F.; Weyhermüller, T.; Wieghardt, K.; Chaudhuri, P. *Inorg. Chem.* **2002**, *41*, 4405.
(9) Khanra, S.; Biswas, B.; Golze, C.; Büchner, B.; Kataev, V.; Weyhermüller, T.; Chaudhuri, P. *Dalton Trans.* **2007**, *4*, 481.
(10) (a) Mukherjee, S.; Weyhermüller, T.; Bill, E.; Chaudhuri, P. *Eur. J. Inorg. Chem.* **2004**, 4209. (b) Paine, T. K.; Weyhermüller, T.; Slep, L. D.; Neese, F.; Bill, E.; Bothe, E.; Wieghardt, K.; Chaudhuri, P. *Inorg. Chem.* **2004**, *43*, 7324. (c) Paine, T. K.; Rentschler, E.; Weyhermüller, T.; Chaudhuri, P. *Eur. J. Inorg. Chem.* **2003**, 3167. (d) Görner, H.; Khanra, S.; Weyhermüller, T.; Chaudhuri, P. *J. Phys. Chem. A* **2006**, *110*, 2587. (e) Khanra, S.; Weyhermüller, T.; Bill, E.; Chaudhuri, P. *Inorg. Chem.* **2006**, *45*, 5911.
(11) Saalfrank, R. W.; Scheurer, A.; Bernt, I.; Heinemann, F. W.; Postnikov, A. V.; Schünemann, V.; Trautwein, A. X.; Alam, M.; Rupp, H.; Müller, P. *Dalton Trans.* **2006**, *23*, 2865.
(12) Takács, A. F.; Neumann, M.; Postnikov, A. V.; Kuepper, K.; Scheurer, A.; Sperner, S.; Saalfrank, R. W.; Prince, K. C. *J. Chem. Phys.* **2006**, *124*, 4503-+

ferromagnetic coupling between the outer manganese ions. Because the manganese star molecule comprises four Mn^{2+} ions ($S = {}^5/_2$ spin state), one expects a giant magnetic net moment of 10 μ_B/formula unit (fu). Although far from trivial by means of chemical manipulation (crystallization with different ligands and/or central ions) or deposition on surfaces, this relatively simple model system allows an exact study of its chemical, electronic, and magnetic properties. To achieve a complete characterization of the manganese star molecule, we apply a number of complementary experimental and theoretical approaches. One appealing finding of our work is a weak ferromagnetic coupling in moderate external fields of a few tesla due to the very weak nature of the intramolecular coupling constants. This leads to a "high-spin" molecule with an overall magnetic moment of 20 μ_B/fu in an ideal case.

This Article is structured as follows. The experimental and theoretical procedures are described in the following section. Later on, the synthesis is described and a structural characterization given. We present a detailed analysis of the magnetic properties by means of SQUID and X-ray magnetic circular dichroism (XMCD) techniques. Whereas the first method tackles the overall magnetic properties of the compound in question, XMCD is well-known for its unique capabilities not only to be an element-specific probe of the magnetization but also to enable the separation into orbital and spin moment.[13,14] The underlying mechanism of X-ray absorption spectroscopy (XAS), furthermore, gains deep insight into the local electronic structure of the Mn^{2+} ions. Besides XAS, the techniques of X-ray photoelectron spectroscopy (XPS) and X-ray emission spectroscopy (XES) are tools of unique precision concerning the analysis of the spatial distribution of the electron and chemical bonding of transition-metal compounds, including molecular magnets.[12,15–17] The latter probes are especially useful in combination with first principles electronic structure calculations, and we will present a detailed analysis of the electronic valence band structure of the manganese star molecule by comparing experimental and theoretical results. Finally, we sum up our main conclusions.

2. Experimental and Theoretical Procedures

2.1. Experimental Methods. 2.1.1. Materials and Physical Measurements. Reagent- or analytical-grade materials were obtained from commercial suppliers and used without further purification. Elemental analyses (C, H, N, and metal) were performed by the Microanalytical Laboratory, Mülheim, Germany. Fourier transform IR spectra of the samples in KBr disks were recorded with a Perkin-Elmer 2000 FT-IR instrument. Magnetic susceptibilities of powdered samples were recorded with a SQUID magnetometer in the temperature range 2−290 K with an applied field of 1 T. Experimental susceptibility data were corrected for their underlying diamagnetism using Pascal's constants. Mass spectra were recorded with either a Finnigan MAT 8200 (electron ionization, EIMS) or a MAT 95 (electrospray, ESI-MS) instrument.

2.1.2. Preparations. The substituted and unsubstituted derivatives of 2-hydroxyphenyl(2-pyridylmethaneimine), HL, were prepared by the Schiff base condensation of 2-pyridylaldehyde (or its derivatives) and 2-aminophenol (or its 2,6-di-*tert*-butyl derivative) using the same protocol. As an example, the protocol for the di-*tert*-butyl derivative is given below.

A solution of 3,5-di-*tert*-butyl-2-aminophenol (5.75 g, 26 mmol) and pyridine-2-aldehyde (2.83 g, 26 mmol) in distilled methanol (400 mL) was stirred at room temperature under argon for 12 h, after which the precipitated yellow solid was separated by filtration and dried in air. Yield: 7.5 g (92%). Purity was checked by gas chromatography (GC; Hewlett-Packard 6890): retention time 23.1 min; column Rtx-5 amine 15m, S-77, detector, FID, temp program 60−310 °C (8 °C/min) ∼95%. EI-MS: *m/z* 310 (61%), 295 (33%), 232 (100%). IR (KBr, cm^{-1}): 3335s, 2992−2865s, 1623s, 1590s, 1577s, 1481s, 1468s, 1438s, 1413s, 1389m, 1363s, 1295m, 1251s, 1190s, 1146s, 1125s, 959s, 881m, 863m, 806m, 780m, 761m, 742m, 683m, 648m. ^1H NMR (400 MHz, $CDCl_3$): 1.313−1.443 (18H, m), 7.290−7.310 (3H, m), 7.742 (2H, m), 8.188−8.208 (1H, d), 8.684 (1H, d), 8.848 (1H, s).

Mononuclear $[Mn^{II}L_2]$ and Their Derivatives. The mononuclear complexes were also prepared very similarly by the reaction of a solution of HL (2 mmol) in acetone (20 mL) with manganese(II) acetylacetonate (0.25 g, 1 mmol) in acetone (30 mL), whereupon the yellow slurry changed its color to deep red. After stirring for 1 h, the red solid was isolated by filtration and washed thoroughly with acetone to yield $[Mn^{II}L_2]$. Yield: ∼50%.

$[Mn^{II}L^H_2]$. Anal. Calcd for $C_{24}H_{18}N_4O_2Mn$ (449.37): C, 64.15; H, 4.04; N, 12.47; Mn, 12.23. Found: C, 64.3; H, 4.1; N, 12.5; Mn, 12.4. EI-MS: *m/z* 449 (81.7%) $[M]^+$, 371 (49.2%) $[M - C_5H_4N]^+$, 252 (100%) $[M - L]^+$, 196 (68.9%) $[L]^+$. X-ray-quality crystals of $[Mn^{II}L^{CH_3}_2]\cdot CH_3OH$ (**1**) were grown from a solution of $[Mn^{II}L^{CH_3}_2]$ in methanol.

$[Mn^{II}_4L^H_6](BF_4)_2\cdot 2CH_3CN\cdot H_2O$ (2). A solution of mononuclear $[Mn^{II}L^H_2]$ (0.45 g, 1 mmol) and $Mn(CH_3COO)_2\cdot 4H_2O$ (0.09 g, 0.33 mmol) in a solvent mixture of acetonitrile/methanol (1:1, 30 mL) was stirred in the presence of air for 0.5 h, and Bu_4NBF_4 (0.96 g/3 mmol) was then added to the deep-colored, nearly black solution. The precipitated red solid was separated by filtration, washed with diethyl ether, and air dried. X-ray-quality crystals were grown by diffusion of diethyl ether into an acetonitrile solution of red $[Mn^{II}_4L^H_6](BF_4)_2$. Yield: 0.22 g (40%). Anal. Calcd for $C_{76}H_{62}B_2F_8Mn_4N_{14}O_7$ (1676.78): C, 54.44; H, 3.73; N, 11.70; Mn, 13.11. Found: C, 54.4; H, 3.6; N, 11.6; Mn, 13.2. IR (KBr, cm^{-1}): 3053, 1585, 1479, 1457, 1298, 1280, 1146, 1083, 1061, 865, 750. ESI-MS: *m/z* 701 (100%) $[M - 2(BF_4)]^{2+}$, 1489 (10%) $[M\text{-}BF_4]^+$.

2.1.3. X-ray Crystallographic Data Collection and Refinement of the Structures. The crystallographic data for $HL^{t\text{-}Bu}$, the mononuclear **1**, and the tetranuclear **2** are summarized in Table 1. A perspective view and selected bond lengths of the $HL^{t\text{-}Bu}$ ligand are presented in Figure 3 and Table 2. Graphite-monochromated Mo Kα radiation (λ = 0.710 73 Å) was used for all three compounds. The crystals of $HL^{t\text{-}Bu}$, **1**, and **2** were fixed with perfluoropolyether onto glass fibers and mounted on a Nonius-

(13) Chen, C. T.; Idzerda, Y. U.; Lin, H.-J.; Smith, N. V.; Meigs, G.; Chaban, E.; Ho, G. H.; Pellegrin, E.; Sette, F. *Phys. Rev. Lett.* **1995**, *75*, 152–155.
(14) Funk, T.; Deb, A.; George, S. J.; Wang, H. X.; Cramer, S. P. *Coord. Chem. Rev.* **2005**, *249*, 3.
(15) Kuepper, K.; Bondino, F.; Prince, K.; Zangrando, M.; Zacchigna, M.; Takacs, A.; Crainic, T.; Matteucci, M.; Parmigiani, F.; Winiarski, A.; Galakhov, V.; Mukovskii, Y.; Neumann, M. *J. Phys. Chem. B* **2005**, *109*, 15667–15670.
(16) Kuepper, K.; Falub, M.; Prince, K.; Galakhov, V.; Troyanchuk, I.; Chiuzbaian, S.; Matteucci, M.; Wett, D.; Szargan, R.; Ovechkina, N.; Mukovskii, Y.; Neumann, M. *J. Phys. Chem. B* **2005**, *109*, 9354–9361.
(17) Kuepper, K.; Kadiroglu, M.; Postnikov, A. V.; Prince, K. C.; Matteucci, M.; Galakhov, V. R.; Hesse, H.; Borstel, G.; Neumann, M. *J. Phys.: Condens. Matter* **2005**, *17*, 4309–4317.

Table 1. Crystal Data and Structure Refinement for $HL^{t\text{-}Bu}$, Complex **1**·CH_3OH, and Complex **2**·$2CH_3CN$·H_2O

	$HL^{t\text{-}Bu}$	complex **1**·CH_3OH	complex **2**·$2CH_3CN$·H_2O
empirical formula	$C_{20}H_{26}N_2O$	$C_{27}H_{26}MnN_4O_3$	$C_{76}H_{62}B_2F_8Mn_4N_{14}O_7$
fw	310.43	509.46	1676.78
temperature (K)	100(2)	100(2)	100(2)
wavelength (Å)	0.71073	0.71073	0.71073
cryst syst	monoclinic	monoclinic	tetragonal
space group	$P2_1/c$	$P2_1/c$	$I4_1/a$
unit cell dimens	a = 16.6521(7) Å	a = 9.1261(4) Å	a = 17.0154(9) Å
	b = 11.1917(5) Å	b = 26.6124(12) Å	b = 17.0154(9) Å
	c = 9.7074(4) Å	c = 10.6470(6) Å	c = 53.619(4) Å
	β = 95.486(5)°	β = 110.09(1)°	$\alpha = \beta = \gamma$ = 90°
vol (Å^3), Z	1800.84(13), 4	2428.5(2), 4	15524.0(16), 8
calcd density (Mg/m^3)	1.145	1.393	1.435
abs coeff (mm^{-1})	0.071	0.580	0.717
F(000)	672	1060	6832
cryst size (mm)	0.11 × 0.10 × 0.02	0.10 × 0.05 × 0.04	0.23 × 0.17 × 0.13
θ range for data collection (deg)	4.44−27.50	7.07−30.97	2.24−26.35
reflns collcd/unique	28 118/4117 [R(int) = 0.0895]	61 457/7593 [R(int) = 0.0520]	53 622/7932 [R(int) = 0.0338]
abs corrn	semiempirical from equiv	not measd	Gaussian, face-indexed
refinement method	full-matrix least squares on F^2	full-matrix least squares on F^2	full matrix least squares on F^2
data/restraints/param	4117/0/215	7593/0/320	7843/0/507
GOF on F^2	1.013	1.035	1.028
final R indices [$I > 2\sigma(I)$]	R1 = 0.0513, wR2 = 0.0957	R1 = 0.0327, wR2 = 0.0758	R1 = 0.0353, wR2 = 0.0930
R indices (all data)	R1 = 0.0865, wR2 = 0.1084	R1 = 0.0445, wR2 = 0.0815	R1 = 0.0571, wR2 = 0.1742
largest diff peak and hole (e/Å^3)	+0.272 and −0.200	+0.373 and −0.222	+0.649 and −0.413

Kappa CCD diffractometer equipped with a cryogenic nitrogen cold stream operating at 100(2) K. Final cell constants were obtained from a least-squares fit of all measured reflections. Intensity data were corrected for Lorentz and polarization effects. The intensity data set of $HL^{t\text{-}Bu}$ and of **2** were corrected for absorption with the use of either the semiempirical method for $HL^{t\text{-}Bu}$ or the Gaussian, face-indexed program for **2**, whereas the data set for **1** was not corrected for absorption. The Siemens *SHELXTL* software package (Sheldrick, G. M. *SHELXTL*; Universität Göttingen: Göttingen, Germany) was used for solution, refinement, and artwork of the structures; the neutral atom scattering factors of the program were used. The structures were solved and refined by direct methods and difference Fourier techniques. Non-hydrogen atoms were refined anisotropically, and hydrogen atoms were placed at calculated positions and refined as riding atoms with isotropic displacement parameters. Split atom models were used to account for disorder of the solvent molecules.

2.1.4. X-ray Spectroscopic Techniques. The soft XAS and XMCD spectroscopy were performed at the elliptically polarizing undulator Beamline 4.0.2 of the Advanced Light Source (ALS), Berkeley, CA.[18] The samples have been mounted into a cryostat equipped with a 6 T superconducting magnet,[19] the sample stage was connected to a pumped helium cryostat, reaching a base temperature of around 5.0 K during the experiments presented here. The measurements at the Mn L edge have been recorded under external magnetic fields of different strength in the total electron yield mode.

The X-ray emission spectra were recorded at the soft X-ray fluorescence end station at the undulator-based Beamline 8.0.1 of the ALS.[20] The excitation energies were set to about 543.9 eV for

Table 2. Selected Bond Lengths (Å) and Angles (deg) for $HL^{t\text{-}Bu}$

O(1)−C(2)	1.3701(18)	N(8)−C(9)	1.273(2)
C(2)−C(3)	1.401(2)	C(9)−C(10)	1.473(2)
C(2)−C(7)	1.404(2)	C(10)−N(11)	1.349(2)
C(3)−C(4)	1.399(2)	C(10)−C(15)	1.388(2)
C(4)−C(5)	1.394(2)	N(11)−C(12)	1.340(2)
C(5)−C(6)	1.388(2)	C(12)−C(13)	1.384(2)
C(6)−C(7)	1.395(2)	C(13)−C(14)	1.389(2)
C(7)−N(8)	1.418(2)	C(14)−C(15)	1.378(2)
O(1)−C(2)−C(3)	119.64(14)	C(6)−C(7)−N(8)	123.92(14)
O(1)−C(2)−C(7)	119.83(14)	C(2)−C(7)−N(8)	115.86(13)
C(3)−C(2)−C(7)	120.53(14)	C(9)−N(8)−C(7)	118.73(13)
C(4)−C(3)−C(2)	116.86(14)	N(8)−C(9)−C(10)	122.50(14)
C(4)−C(3)−C(16)	121.37(14)	N(11)−C(10)−C(15)	123.35(15)
C(2)−C(3)−C(16)	121.77(14)	N811)-C(10)−C(9)	113.80(13)
C(5)−C(4)−C(3)	124.06(15)	C(15)−C(10)−C(9)	122.84(14)
C(6)−C(5)−C(4)	117.41(14)	C(12)−N(11)−C(10)	116.93(14)
C(6)−C(5)−C(20)	120.23(14)	N(11)−C(12)−C(13)	123.46(16)
C(4)−C(5)−C(20)	122.33(14)	C(12)−C(13)−C(14)	118.69(16)
C(5)−C(6)−C(7)	120.94(15)	C(15)−C(14)−C(13)	118.91(15)
C(6)−C(7)−C(2)	120.18(14)	C(14)−C(15)−C(10)	118.64(15)
O(1)···N(11a) (intermol.)	2.90	O(1)···N(8) (intramol.)	2.71

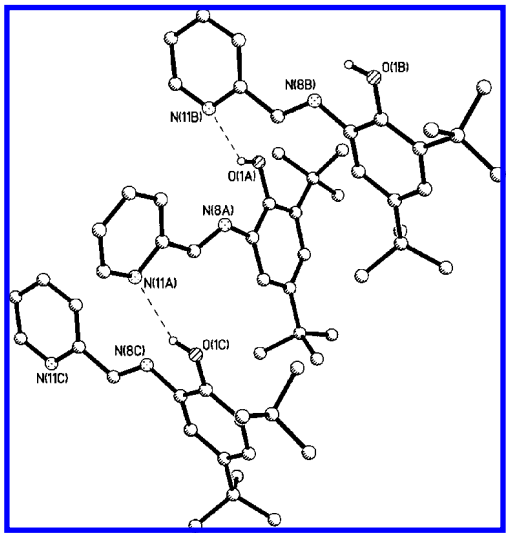

Figure 3. Molecular structure of the 2,6-di-*tert*-butyl-substituted ligand $HL^{t\text{-}Bu}$.

(18) Young, A. T.; Martynov, V.; Padmore, H. A. *J. Electron Spectrosc. Relat. Phenom.* **1999**, *103*, 885.
(19) Funk, T.; Friedrich, S.; Young, A.; Arenholz, E.; Cramer, S. P. *Rev. Sci. Instrum.* **2002**, *73*, 1649.
(20) Jia, J. J.; Callcott, T. A.; Yurkas, J.; Ellis, A. W.; Himpsel, F. J.; Samant, M. G.; Stöhr, G.; Ederer, D. L.; Carlisle, J. A.; Hudson, E. A.; Terminello, L. J.; Shuh, D. K.; Perera, R. C. C. *Rev. Sci. Instrum.* **1995**, *66*, 1394–1397.

the O K edge and 639.1 eV for the Mn L_3 edge, with an overall resolution (beamline plus spectrometer) set to around 1 eV for the XES measurements.

The complementary XPS measurements were performed at the Department of Physics, University of Osnabrück, Osnabrück, Germany, using a PHI 5600CI multitechnique spectrometer with monochromatic Al Kα = 1486.6 eV radiation of 0.3 eV at full-width at half-maximum. The overall resolution of the spectrometer is 1.5% of the pass energy of the analyzer, 0.35 eV in the present case. The XES and XPS measurements were performed at room temperature.

2.2. Theoretical Section. 2.2.1. DFT Calculations. The electronic structure calculations have been done within the density functional theory (DFT) paradigm, technically using the Siesta calculation method[21] and band structure code.[22] This implementation uses norm-conserving pseudopotentials, which were in our case generated within the Troullier−Martins scheme.[23] The pseudopotential for manganese has been constructed in the $4s^1 3p^6 3d^5 4f^0$ configuration of the valence states, with corresponding pseudoionization radii 2.00, 1.90, 1.90, and 1.50 Bohr in s through f channels. The parameters of other pseudopotentials were as follows (charge configuration followed by the corresponding radius in Bohr): H $1s^1(1.25)2p^0(1.25)3d^0(1.25)4f^0(1.25)$; C $2s^2(1.25)2p^2(1.25)3d^0(1.25)4f^0(1.25)$; N $2s^2(1.25)2p^3(1.25)3d^0(1.25)4f^0(1.25)$; O $2s^2(1.15)2p^4(1.15)3d^0(1.15)4f^0(1.15)$.

As for (atom-centered and strictly confined) basis functions, they were constructed as pseudoatomic orbitals for given pseudopotentials, see, e.g., refs 24 and 25. They have been taken in (at least) double-ζ quality, adding polarization orbitals for O and N (which are responsible for the chemical bonding with Mn) and extending up to triple-ζ in the Mn 3d channel (and adding polarization orbitals to Mn 4s). The spin-density isosurface plots were prepared with the *XCrySDen* software.[26]

2.2.2. Multiplet Calculations. The XAS and MCD line shapes of the Mn $L_{2,3}$ edges were simulated using the TT multiplet simulation program.[27,28] First, the energy levels of the initial ($2p^6 3d^5$) and final ($2p^5 3d^6$) states were calculated in spherical (O_3) symmetry. The parameters include the spin−orbit coupling of the 2p core and 3d valence band electrons, the 3d3d as well as the 2p3d Slater integrals in the initial and final states, which are summarized in Table 3. The d−d and p−d integrals were reduced to 90% of the values[29] shown in the table, whereas the spin−orbit parameters were not reduced. Then a cubic crystal field (O_h symmetry) of 0.6 eV strength and an internal exchange field of 0.05 eV were considered in the crystal-field approach. Finally admixtures of other configurations, namely, a charge-transfer configuration $3d^6\underline{L}$, were considered by performing additional monopole calculations for the initial (between $2p^6 3d^5$ and $2p^6 3d^6\underline{L}$) and final (between $2p^5 3d^6$ and $2p^5 3d^7\underline{L}$) states. The energy difference between the two configurations $E(2p^6 3d^5) - E(2p^6 3d^6\underline{L})$ = Δ was set to 9.0 eV, which corresponds to the value found for MnO.[30] For a comparison with the experiment, the lifetime broadening of the 2p core hole and the resolution of the spectrometer were taken into account.

Table 3. Slater Integrals Used for the Multiplet Simulations of the Mn $L_{2,3}$ XA and MCD Spectra[a]

	$2p^6 3d^5$ initial state	$2p^5 3d^6$ final state	$2p^6 3d^6 L$ initial state	$2p^5 3d^7 L$ final state
Slater Integrals				
F^2_{3d3d}	10.316	11.155	9.073	9.972
F^4_{3d3d}	6.414	6.943	5.591	6.157
F^2_{2p3d}		6.321		5.653
G^1_{2p3d}		4.606		4.059
G^3_{2p3d}		2.618		2.305
Spin−Orbit Coupling				
LS_{2p}		6.846		6.847
LS_{3d}	0.040	0.053	0.035	0.046

[a] For the calculations, the d−d and p−d integrals were reduced to 90% of the values shown in the table, whereas the spin−orbit parameters were not reduced.

3. Results and Discussion

3.1. Molecular Structures of $HL^{t\text{-}Bu}$ and $[MnL^{CH_3}{}_2]$. The ligand 2-hydroxyphenyl(2-pyridylmethaneimine), HL^R, was prepared according to a modified procedure reported in the literature by the Schiff base condensation of 2-pyridylaldehyde (or its 2-methyl derivative) and 2-aminophenol (or its 2,6-di-*tert*-butyl derivative). The purity of the ligand was checked by liquid chromatography to be ca. 99.0%. The IR, ^{1}H NMR, and MS results are in agreement with the literature data, and hence no further discussion is necessary. To gain insight into the metrical parameters of the ligand, we have determined the structure of the ligand in its di-*tert*-butyl form by X-ray diffractometry. The structure of the ligand $HL^{t\text{-}Bu}$ in the solid state is shown in Figure 3.

The X-ray analysis of single crystals of $HL^{t\text{-}Bu}$, performed at 100 K, reveals a strong intramolecular hydrogen bonding between the phenolic hydroxyl group O(1) and the imine nitrogen N(8) with O(1)H···N(8) at 2.71 Å, whereas an intermolecular hydrogen bonding between the O(1) and the pyridine nitrogen N(11a) of the neighboring molecule at O(1)···N(11a) 2.90 Å can be envisaged. It is noteworthy that the C(7)−N(8) distance with 1.418(2) Å is of double-bond character, as expected. The bond lengths and angles for $HL^{t\text{-}Bu}$, listed in Table 2, seem reasonable and do not warrant any special discussion. Methanolic solutions of HL^R were treated with manganous(II) salts, in a 2:1 ratio under argon in the presence of a base, and the solution was heated to reflux to yield the mononuclear precursor **1**. In the IR spectrum of the complex, the OH stretching vibrations of the free ligand are missing, indicating the coordinated phenoxide groups. EI-MS spectrometry was helpful in detecting the mononuclear nature for $[MnL^H{}_2]^0$. The molecular ion peak at *m/z* 449 (81.7%), together with the fragments at *m/z* 371 (49.2%), 252 (100%), 196 (68.9%), 173 (24.2%), 120 (35%), and 109 (26.3%), clearly indicates the identity of the precursor $[MnL^H{}_2]^0$. Because the manganese precursor,

(21) Soler, J. M.; Artacho, E.; Gale, J. D.; García, A.; Junquera, J.; Ordejón, P.; Sánchez-Portal, D. *J. Phys.: Condens. Matter* **2002**, *14*, 2745–2779.
(22) URL: http://www.uam.es/siesta.
(23) Troullier, N.; Martins, J. L. *Phys. Rev. B* **1991**, *43*, 1993–2006.
(24) Junquera, J.; Paz, Ó.; Sánchez-Portal, D.; Artacho, E. *Phys. Rev. B* **2001**, *64*, 235111.
(25) Sánchez-Portal, D.; Artacho, E.; Soler, J. M. *J. Phys.: Condens. Matter* **1996**, *8*, 3859–380.
(26) Kokalj, A. *Comput. Mater. Sci.* **2003**, *28*, 155.
(27) de Groot, F. M. F. *J. Electron Spectrosc. Relat. Phenom.* **1994**, *67*, 529.
(28) de Groot, F. M. F. *Coord. Chem. Rev.* **2005**, *249*, 31.
(29) Uozumi, T.; Okada, K.; Kotani, A.; Zimmermann, R.; Steiner, P.; Hüfner, S.; Tezuka, Y.; Shin, S. *J. Electron Spectrosc. Relat. Phenom.* **1997**, *83*, 9.
(30) Okada, K.; Kotani, A. *J. Phys. Soc. Jpn.* **1992**, *61*, 4619.

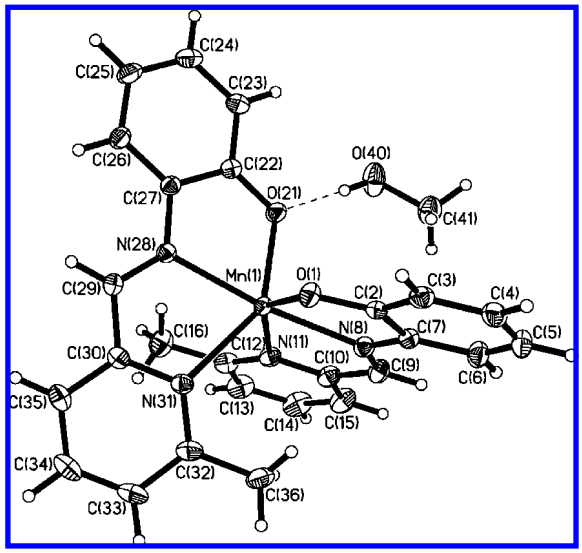

Figure 4. ORTEP diagram of the mononuclear **1**.

Table 4. Selected Bond Lengths (Å) and Angles (deg) for **1**

Mn(1)−O(1)	2.1197(9)	N(8)−C(9)	1.2837(15)
Mn(1)−O(21)	2.1485(8)	N(28)−C(29)	1.2860(15)
Mn(1)−N(8)	2.2249(10)		
Mn81)−N(28)	2.2287(10)		
Mn(1)−N(31)	2.3283(10)		
Mn(1)−N(11)	2.4012(10)		
O(1)−Mn(1)−O(21)	101.43(4)	N(8)−Mn(1)−N(31)	114.39(4)
O(1)−Mn(1)−N(8)	75.55(4)	N(28)−Mn(1)−N(31)	71.61(4)
O(21)−Mn(1)−N(8)	100.38(3)	O(1)−Mn(1)−N(11)	145.06(3)
O(1)−Mn(1)−N(28)	99.80(3)	O(21)−Mn(1)−N(11)	93.71(3)
O(21)−Mn(1)−N(28)	74.56(3)	N(8)−Mn(1)−N(11)	70.82(4)
N(8)−Mn(1)−N(28)	172.51(4)	N(28)−Mn(1)−N(11)	114.60(4)
O(1)−Mn(1)−N(31)	96.02(3)	N(31)−Mn(1)−N(11)	89.47(4)
O(21)−Mn(1)−N(31)	144.04(3)		

prepared in a different way, has been reported[31] without any structural parameters, we grew single crystals of the compound with the 2-methyl derivative (Figure 2) of the ligand (HL^{CH_3}) for the structure determination. Figure 4 shows the ORTEP diagram for the structure of compound $[Mn_2L^{CH_3}]$. Selected bond lengths and angles are summarized in Table 4.

The overall geometry around the manganese atom Mn(1) is best described as a distorted octahedron with two cis-positioned oxygens O(1) and O(21) of the phenolate groups arising from two different ligands; the two tridentate ligands are found to be almost planar and perpendicular to one another. A methanol molecule of crystallization is hydrogen bonded to O(21) with O(21)···HO(40) at 2.702 Å. The pyridine and the phenyl rings of the ligands are not strictly parallel, with an average separation of 4.3 Å. There are no other remarkable features in the structure of $[Mn_2L^{CH_3}]^0$. The bond lengths with average Mn(1)−O at 2.134(1) and Mn(1)−N at 2.296 Å are consistent with those typical for high-spin manganese(II) compounds.[32] This assignment is also complemented by the magnetic susceptibility measurements (20−290 K), which exhibit a temperature-independent magnetic moment μ_{eff} of 5.90 ± 0.02 μ_B, resulting from a high-spin d^5 electron configuration. The structure is comparable to the reported[33] $[Fe^{III}L^{H}_2]ClO_4 \cdot H_2O$ and $[Fe^{III}L^{H}_2]PF_6 \cdot CH_3OH$.

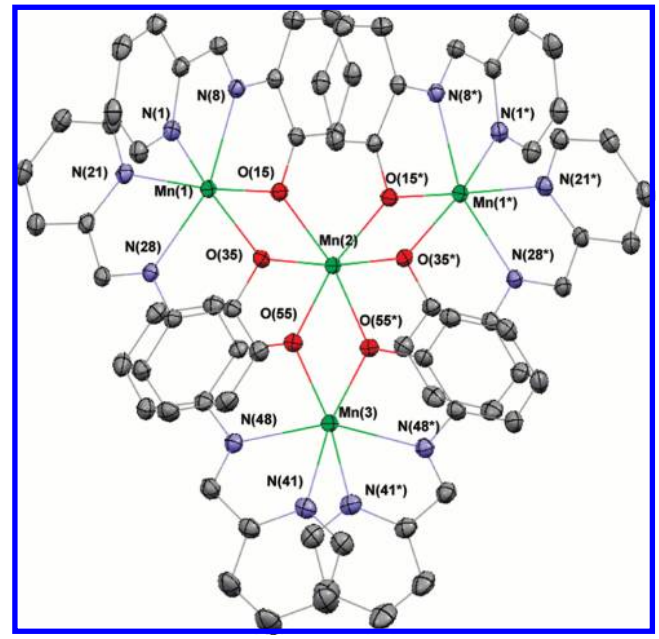

Figure 5. Molecular structure of the cation in complex **2**.

Table 5. Selected Bond Lengths (Å) and Angles (deg) for **2**

Mn(1)···Mn(2)	3.286	Mn(3)···Mn(2)	3.322
Mn(1)−O(15)	2.139(14)	Mn(2)−O(55)	2.17(14)
Mn(1)−O(35)	2.144(14)	Mn(2)−O(55)	2.17(14)
Mn(1)−N(28)	2.214(2)	Mn(2)−O(15)	2.181(14)
Mn(1)−N(8)	2.223(2)	Mn(2)−O(15)	2.181(14)
Mn(1)−N(1)	2.288(2)	Mn(2)−O(35)	2.186(14)
Mn(1)−N(21)	2.313(2)	Mn(2)−O(35)	2.186(14)
Mn(3)−O(55)	2.141(14)	N(50)−Mn(3)−N(42)	143.56(11)
Mn(3)−O(55)	2.247(14)	N(10)−Mn(1)−N(2)	141.7(12)
Mn(3)−N(48)	2.226(2)	O(15)−Mn(1)−O(35)	82.00(5)
Mn(3)−N(48)	2.226(2)	O(55)−Mn(3)−O(55)	79.81(8)
Mn(3)−N(41)	2.337(2)	O(55)−Mn(2)−O(55)	78.55(7)
Mn(3)−N(41)	2.337(2)	O(15)−Mn(2)−O(15)	93.68(8)
		O(55)−Mn(2)−O(15)	168.54(5)
		Mn(1)−O(15)−Mn(2)	99.07(6)

3.2. Molecular Structure of 2. The structure consists of discrete tetranuclear dications $[Mn_4L_6]^{2+}$, tetrafluoroborate anions, acetonitrile, and water as solvent molecules of crystallization. A view of the entire complex cation is given in Figure 5.

Relevant bond distances and angles are listed in Table 5. The complex cation in **2** can be described as three neutral $[MnL^{H}_2]^0$ units acting as bidentate ligands through the cis-disposed phenolate oxygens for the central Mn(2), yielding the central $Mn(2)O_6$ core. The three peripheral manganese atoms Mn(1), Mn(1*), and Mn(3) form an isosceles triangular arrangement with the centrally situated Mn(2) atom, as schematically shown in the left panel of Figure 10, with corresponding Mn−Mn distances. The labeling of corresponding interaction parameters (to be discussed below) is introduced in the right panel of Figure 10. The bridging plane

(31) Reddig, N.; Triller, M. U.; Pursche, D.; Rompel, A.; Krebs, B. *Z. Anorg. Allg. Chem.* **2002**, *628*, 2458.
(32) *Comprehensive Coordination Chemistry*; Wilkinson, G., Ed.; Pergamon: Oxford, U.K., 1987; Vol. *4*.
(33) (a) Hayami, S.; Gu, Z.; Shiro, M.; Einaga, Y.; Fujishima, A.; Sato, O. *J. Am. Chem. Soc.* **2000**, *122*, 7126. (b) Juhsz, G.; Hayami, S.; Sato, O.; Maeda, Y. *Chem. Phys. Lett.* **2002**, *364*, 164.

comprising the Mn_2O_2 atoms is strictly planar for Mn(3) due to the imposed 2-fold symmetry, whereas the mean deviation for the atoms involving Mn(1)O(35)Mn(2)O(15) is only 0.019 Å from the mean plane, thus lending the tetranuclear cation a propeller shape, as is also evidenced by the dihedral angles of 93.5° and 84.7° between the planes involving Mn(2)Mn(3)O_2/Mn(2)Mn(1)O_2 and Mn(2)Mn(1)O_2/Mn(2)-Mn(1*)O_2, respectively.

All apical manganese atoms, Mn(1), Mn(3), and Mn(1*), are coordinated to four nitrogen atoms [pyridine nitrogens N(1) and N(21) and azomethine nitrogens N(8) and N(28) for Mn(1)] and two phenolate oxygens, O(15) and O(35), resulting in a six-coordinated MnN_4O_2 core, which is attained by ligation of two deprotonated ligands to each of the manganese atoms Mn(1), Mn(3), and Mn(1*). Although Mn(1) and Mn(3) are crystallographically independent, their structural parameters are comparable. The Mn−N bond lengths, as expected, are longer than the corresponding Mn−O distances; on the other hand, Mn−N(pyridine) distances are longer than the Mn−N(azomethine) bond lengths. The Mn−O(phenoxide) at average 2.141 Å and the Mn−N at average 2.267 Å fall well within the ranges that are considered as normal covalent bonds for high-spin d^5 Mn^{II} ions and are very similar to those for the mononuclear **1**. All cis angles at the apical manganese centers deviate from the ideal 90°, with the smallest for Mn(1) and Mn(2) being 72.14(6) and 71.65(6)° for the cis angles N(8)−Mn(1)−N(1) and N(48)−Mn(3)−N(41), respectively, indicating large angular distortions of the coordination environments. The central manganese atom Mn(2) is surrounded by an almost perfect octahedron (maximum deviation of the twist angles between the octahedral faces being 6°) of six phenolato oxygen atoms O(15), O(35), and O(55) and their equivalents. The angle at the bridging phenolate oxygen, Mn−O(phenolate)−Mn, varies only between 98.75(6)° and 100.82(6)°. The Mn(2)−O distance of average 2.179 Å is significantly longer than the trivalent Mn−O distances, ca. 2.00 Å, indicating that Mn(2) is in a lower oxidation state than III+. That the central Mn(2) ion must be ascribed to a II+ (high-spin d^5) oxidation is borne out by the facts that (i) two tetrafluoroborate anions are present for maintaining the electroneutrality of the dicationic $[Mn_4L_6]^{2+}$ complex and (ii) the magnetic data can only be simulated by considering an $S_{Mn} = {}^5/_2$ for the central Mn(2) center. The molecules in the crystal are well-separated from each other, with the shortest Mn···Mn distance between neighboring complexes being 10.34 Å. The structural parameters are very similar to those reported[31,34] recently for $[Mn_4L_6](BPh_4)_2$ and $[Mn_4L_6](ClO_4)_2$ complexes.

3.3. Magnetic Susceptibility Measurements. Magnetic susceptibility data for the polycrystalline sample of the tetranuclear complex **2** were collected in the temperature range 2−290 K in an applied magnetic field of 1 T. The magnetic moment μ_{eff}/molecule for **2** of 11.75 μ_B ($\chi_M T$ = 17.257 cm^3 K mol^{-1}) at 290 K increases monotonically with decreasing temperature until the value of μ_{eff} = 12.428 μ_B ($\chi_M T$ = 19.31 cm^3 K mol^{-1}) is attained at 10 K, below which μ_{eff} decreases, reaching a value of 7.99 μ_B ($\chi_M T$ = 7.98 cm^3 K mol^{-1}) at 2 K. This temperature dependence indicates an overall ferromagnetic coupling. We use the Heisenberg spin Hamiltonian in the form

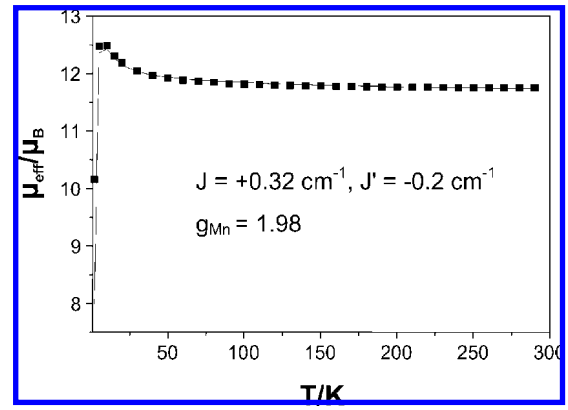

Figure 6. Plot of μ_{eff} vs temperature (T) for complex **2**.

$$H = -2J(S_2 \cdot S_1 + S_1^* \cdot S_2) - 2J' S_2 \cdot S_3 \qquad (1)$$

for an isotropic exchange coupling with $S_1 = S_2 = S_3 = S_1^* = {}^5/_2$ for **2**. The experimental data as the effective magnetic moments μ_{eff} vs temperature (T) are displayed in Figure 6. The experimental magnetic data were simulated using a least-squares computer program[35] with a full-matrix diagonalization approach, and the solid line in Figure 6 represents the simulation.

The magnetic analysis was carried out using a "two-J" model corroborating with two different prevailing bridging angles, Mn(1)−O−Mn(2) at 98.9° and Mn(2)−O−Mn(3) at 100.8°, depicted in Figure 10. In order to avoid overparametrization, we have set the single ion axial zero-field splitting, D, to zero and considered a unique isotropic g factor to evaluate the magnitude for the main parameters J and J' (see Figure 10).

The best-fit parameters are $J = +0.32$ cm^{-1} and $J' = -0.2$ cm^{-1} with g_{Mn} = 1.98. It is worth mentioning that the experimental data can also be simulated with a "one-J" model, leading to the fit parameters $J = J' = +0.2$ cm^{-1}, g_{Mn} = 1.98, and $\Theta = -0.2$ K. Because the nature of the signs of the exchange parameters corroborates with the Mn−O−Mn angle correlation and the Mn(2)···Mn(1) and Mn(2)···Mn(3) separations, we prefer the two-J model. To verify further the weak ferromagnetic interactions, variable-temperature variable-field (VTVH) measurements have been performed with 1, 4, and 7 T in the temperature range of 1.95−290 K, depicted in Figure 7.

The magnetization increases more rapidly than that of the uncoupled system with the saturation magnetization at 10 N$g\beta$, confirming the ferromagnetic interaction. At very low temperatures (2−3 K), there are small drops in the magnetization curves. That the saturation occurs much more slowly indicates the weakness and the presence of additional antiferromagnetic interactions, supporting further our "two-

(34) Gao, E.-Q.; Bai, S.-Q.; Zheng, H.; Yan, C.-H. *Inorg. Chem.* **2005**, *44*, 677.

(35) Bill, E. Max-Planck-Institut für Bioanorganische Chemie, Mülheim an der Ruhr, Germany, 2005.

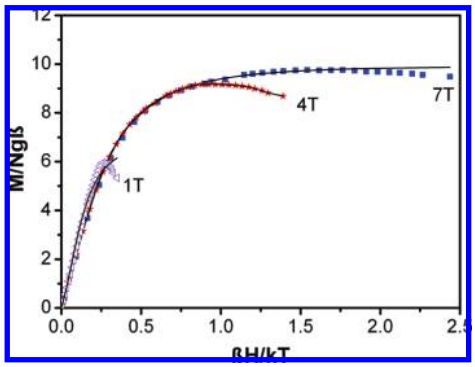

Figure 7. VTVH plots for complex **2** at 1, 4, and 7 T in the temperature range 2−290 K.

J' model. The parameters evaluated from the VTVH measurements are $J = +0.47$ cm^{-1}, $J' = -0.19$ cm^{-1}, and $g_{Mn} = 1.98$, which are very similar to those from the isofield measurements. So, the high-spin Mn^{II} centers with $S = {}^5/_2$ in **2** exhibit weak dominant ferromagnetic coupling, yielding a "high-spin" molecule with an $S_t = 10$ ground state. Because of the weak nature of the couplings, the molecule shows a complicated low-lying magnetic structure with the ground state not well-separated from the upper-lying states. Accordingly, the measured magnetization has more contributions from excited states of lower spins than from the ground-state spin. The above discussion is qualitatively valid, although we have ignored the zero-field-splitting effects. The magnetic behavior of **2** is similar to that reported for the analogous perchlorate salt, for which the authors used a "one-J" model together with the Weiss constant Θ (see above).[34] Because of negligible zero-field-splitting and intermolecular effects, magnetic moments extracted from XMCD measurements, to be discussed in the next section, can nicely be fitted by a Brillouin magnetization curve.

Exchange coupling constants in bis(μ-phenoxo)-bridged dimanganese(II) complexes published,[36] the number of which is much smaller than that of the diferric(III) analogues, have been found to be very small, lying in a small range of +0.2 to −1.88 cm^{-1}. The angle at the bridging phenoxide oxygen is expected to be important because this affects the nature of σ and π overlap between the manganese magnetic orbitals and the oxygen p_x, p_y, and p_z orbitals that mediate the exchange interaction. Such correlations between the exchange integral J and the M−O−M bridging angle[37,38] have been tried to be established for nickel(II) and copper(II), and the exchange interaction changes from antiferromagnetic to ferromagnetic at an angle, in most cases, below 98°. However, such magnetostructural analyses for the coupled manganese(II) and iron(III) complexes are far more intrinsically difficult because of the larger number of magnetic orbitals and exchange pathways involved for high-spin d^5 ions. Nevertheless, some semiempirical correlations between J and the bridging parameters have been attempted to be established for diiron(III) complexes[39] with phenoxo, alkoxo, and hydroxo bridges. It is notable that all diiron(III) complexes display antiferromagnetic interactions except one whose ferromagnetic coupling[40] has been attributed to the distortion of the coordination geometry, based on extended Hückel molecular orbital calculations. That the exchange interactions for the ferric complexes are much stronger than those for the isoelectronic manganese(II) complexes reflects the stronger covalency of the iron(III)−ligand bonds in comparison to that for the manganese(II)−ligand bonds. All reported six-coordinated bis(μ-phenoxo)-bridged dimanganese(II)[36] complexes exhibit weak antiferromagnetic interactions. However, only one five-coordinated bis(μ-phenoxo)-dimanganese(II) compound has been found to be very weakly ferromagnetically coupled ($J = +0.24$ cm^{-1}).[36a] Overall, the exchange parameter J, both ferro- and antiferromagnetic exchange, is found to be very low for all reported manganese(II) complexes including the present complex **2** because ineffective t_{2g}−t_{2g} π pathways dominate the exchange; this weak nature is further augmented by the deviation of the metal geometry toward a trigonal prism (D_{3h}). Similar star-shaped $Fe^{III}{}_4O_6$ motifs[11,12,41] have been found to be antiferromagnetically coupled, yielding a ground state of $S_t = {}^{10}/_2$.

3.4. XMCD. The top panel of Figure 8 displays the X-ray absorption spectra (dotted lines) excited with 90% left and right circularly polarized light in an external magnetic field of 5 T.

The thinner solid lines represent the corresponding Mn^{2+} charge-transfer multiplet calculations. The spectra have been calculated at $T = 5$ K using the multiplet program developed by Thole, which is based upon the codes of Cowan and

(36) (a) Chang, H.-R.; Larsen, S. C.; Boyd, P. D. W.; Pierpont, C. G.; Hendrickson, D. N. *J. Am. Chem. Soc.* **1988**, *110*, 4565. (b) Yu, S.-B.; Wang, C.-P.; Day, E. P.; Holm, R. H. *Inorg. Chem.* **1991**, *30*, 4067. (c) Gallo, E.; Solari, E.; Re, N.; Floriani, C.; Chiesi-Villa, A.; Rizzoli, C. *J. Am. Chem. Soc.* **1997**, *119*, 5144. (d) Blanchard, S.; Blondin, G.; Riviére, E.; Nierlich, M.; Girerd, J.-J. *Inorg. Chem.* **2003**, *42*, 4568. (e) Alexiou, M.; Dendrinou-Samara, C.; Karagianni, A.; Biswas, S.; Zaleski, C. M.; Kampf, J.; Yoder, D.; Penner-Hahn, J. E.; Pecoraro, V. L.; Kessisoglou, D. P. *Inorg. Chem.* **2003**, *42*, 2185. (f) Coucouvanis, D.; Greiwe, K.; Salifoglou, A.; Challen, P.; Simolpoulos, A.; Kostikas, A. *Inorg. Chem.* **1988**, *27*, 593. (g) Qian, M.; Gou, S.; Chantrapromma, S.; Raj, S. S. S.; Fun, H.-K.; Zeng, Q.; Yu, Z.; You, X. *Inorg. Chim. Acta* **2000**, *305*, 83.

(37) (a) Crawford, V. H.; Richardson, H. W.; Wasson, J. R.; Hodgson, D. J.; Hatfield, W. E. *Inorg. Chem.* **1976**, *15*, 2107. (b) Hodgson, D. J. *Prog. Inorg. Chem.* **1975**, *19*, 173.

(38) (a) Nanda, K. K.; Thompson, L. K.; Bridson, J. N.; Nag, K. *J. Chem. Soc., Chem. Commun.* **1994**, 1337. (b) Halcrow, M. A.; Sun, J.-S.; Huffman, J. C.; Christou, G. *Inorg. Chem.* **1995**, *34*, 4167. (c) Clemente-Juan, J. M.; Chansou, B.; Donnadieu, B.; Tuchagues, J. P. *Inorg. Chem.* **2000**, *39*, 5515. (d) Mukherjee, S.; Weyhermüller, T.; Bothe, E.; Wieghardt, K.; Chaudhuri, P. *Eur. J. Inorg. Chem.* **2003**, 863. (e) Paine, T. K.; Rentschler, E.; Weyhermüller, T.; Chaudhuri, P. *Eur. J. Inorg. Chem.* **2003**, 3167. (f) Fondo, M.; Garca-Deibe, A. M.; Ocampo, N.; Sanmartin, J.; Bermejo, M. R.; Llamas-Saiz, A. L. *Dalton Trans.* **2006**, 4260. (g) Chaudhuri, P.; Wagner, R.; Weyhermüller, T. *Inorg. Chem.* **2007**, *46*, 5134.

(39) (a) Gorun, S. M.; Lippard, S. *J. Inorg. Chem.* **1991**, *30*, 1625. (b) Weihe, H.; Güdel, H. U. *J. Am. Chem. Soc.* **1997**, *119*, 6539. (c) Werner, R.; Ostrovsky, S.; Griesar, K.; Haase, W. *Inorg. Chim. Acta* **2001**, *326*, 78.

(40) Snyder, B. S.; Patterson, G. S.; Abrahamson, A. J.; Holm, R. H. *J. Am. Chem. Soc.* **1986**, *111*, 5214.

(41) (a) Barra, A. L.; Caneschi, A.; Cornia, A.; Fabrizi de Biani, F.; Gatteschi, D.; Sangregorio, C.; Sessoli, R.; Sorace, L. *J. Am. Chem. Soc.* **1999**, *121*, 5302. (b) Saalfrank, R. W.; Scheurer, A.; Bernt, I.; Heinamann, F. W.; Postnikov, A. V.; Schünemann, V.; Trautwein, A. X.; Alam, M. S.; Rupp, H.; Müller, P. *Dalton Trans.* **2006**, 2865. and references cited therein.

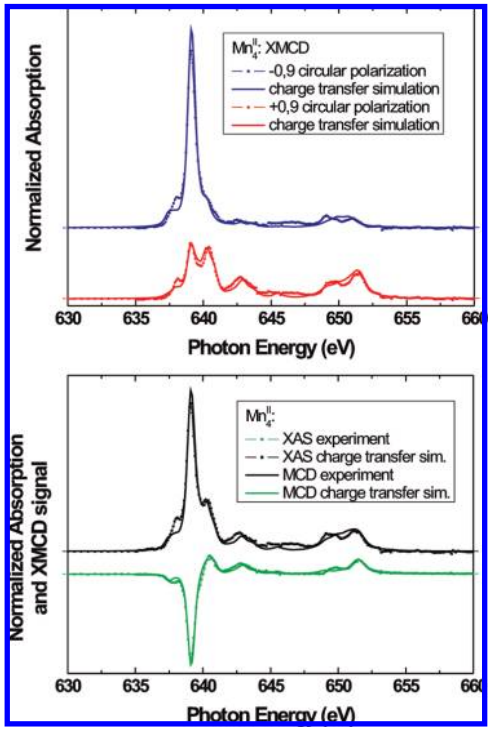

Figure 8. Left and right polarized X-ray absorption spectra recorded in an external magnetic field of 5 T at a temperature of 5 K (top panel) and the corresponding XAS and XMCD signals (bottom panel). The XMCD signal has been normalized to 100% circular polarization. The experimental results are compared with corresponding charge-transfer mulitiplet calculations; we used an octahedral crystal field of 0.6 eV strength.

Butler.[27,28,42,43] In a first step, the Slater integrals and the spin−orbit couplings were calculated in spherical symmetry, these are summarized in Table 3. Then a cubic crystal field (10 Dq) and an external magnetic field of $\mu_B H = 0.05$ eV along the z direction were applied. Finally, the mixing of the $3d^5$ with $3d^6$ charge-transfer states was considered by introducing the energy difference between the two configurations, $\Delta = E(3d^6\underline{L}) - E(3d^5)$. Scanning through the parameter room of 10 Dq and Δ, we find an almost perfect agreement between the experimental and theoretical spectra with 10 Dq = 0.6 eV and $\Delta = 9.0$ eV (Figure 8). In order to enable a direct comparison between experiment and simulation, the calculated spectra have been normalized to 90% circular polarization plus 10% z-polarized absorption ($q = 0$ transitions), for both left and right circularly polarized light. Furthermore, the calculated spectra have been convoluted with the overall experimental resolution (lifetime broadening + spectrometer resolution).

The bottom panel of Figure 8 shows the sum (XAS) and the difference (MCD) of the dichroic XAS spectra displayed in the top panel of Figure 8. The Mn $L_{2,3}$ XAS consists of a shoulder at about 638.0 eV, a main peak at 639.0 eV, and two further shoulders located around 640 and 642.5 eV, respectively. These features represent the excitations originating from the Mn $2p_{3/2}$ core level, followed by the excitations from the Mn $2p_{1/2}$ core level around 649.0 and 651.5 eV. The XAS, sensitive to the chemical environment of the absorbing atom, clearly reflects a pretty ionic Mn^{2+} valence state. From the charge-transfer multiplet simulations, we can extract a 93.8% $3d^5$ and 6.2% $3d^6\underline{L}$ configuration. It is noted that, although only ∼6% charge-transfer states are involved, the charge-transfer multiplet simulation leads to a significant improvement as compared to a simple ligand-field simulation. This especially accounts for the intensity and energetic position of the shoulders between the Mn L_2 and Mn L_3 main peaks.

Moreover, XAS is a direct probe of the local crystal-field environment (strength) around the absorbing manganese atom; with the help of our charge-transfer multiplet calculations, we determine an octahedral crystal field of 0.6 eV strength. In spite of the structural characterization revealing the octahedral environment to be somewhat distorted, this is a good estimation of the average crystal-field strength, present around the manganese atoms. In order to extract the spin and orbital magnetic moments, we applied the sum rules as developed by Chen et al.[13] From the experimental data, we evaluate a spin moment $m_{spin} = 12.35\ \mu_B$/fu (3.09 μ_B/manganese atom) and an orbital moment of $m_{orb} = 0.36\ \mu_B$/fu (0.09 μ_B/atom). From the ground state of the charge-transfer multiplet calculations, we calculate $m_{spin} = 5.00\ \mu_B$/atom and $m_{orb} = 0.00\ \mu_B$/atom. If we apply the sum rules to the theoretical spectra, we extract $m_{spin} = 3.59\ \mu_B$/atom and $m_{orb} = 0.02\ \mu_B$/atom. This implies an error in the spin sum rule due to the effect of the core hole Coulombic interactions that mix the character of the L_3 and L_2 edges. This error is estimated from the calculations to be 3.59/5.00 = 0.72. This value is close to that obtained for a crystal-field calculation of a Mn^{2+} ion with 10 Dq = 1.5 eV.[44] It is noted that the variations of these values (as well as the error) with 10 Dq are small and that in the case of a high-spin $3d^5$ ground state also the spin−orbit coupling has no influence on the sum rule.[45]

This correction factor is only valid if the L_3 to L_2 splitting is sufficiently large so that no considerable L_3−L_2 mixing is present[44] as in the present case. Considering the sum rules and the correction factor for the spin sum rule, we yield a spin moment of $m_{spin} = 17.65\ \mu_B$/fu and a small orbital moment of $m_{orb} = 0.36\ \mu_B$/fu for the "manganese star" molecule under an external field of 5 T and at a temperature of 5 K.

Moreover, we analyzed the magnetization behavior by performing XMCD measurements at a number of different external fields (Figure 9). Table 6 lists the results. Because we have found in section 3.3 that effects from zero-field splitting or intramolecular interactions are negligible, one can nicely extract the (theoretical) magnetization curve by fitting the experimental data with the help of a Brillouin function using an uncoupled $S = {}^5/_2$ as the spin ground state for the "manganese star" molecule (Figure 9).[34,46] The experimental data are in good agreement with a Brillouin

(42) Butler, P. H. *Point Group Symmetry, Applications, Methods and Tables*; Plenum: New York, 1981.
(43) Cowan, R. D. *The Theory of Atomic Structure and Spectra*; University of California Press: Berkeley, CA, 1981.
(44) Termamura, Y.; Tanaka, A.; Jo, T. *J. Phys. Soc. Jpn.* **1996**, *65*, 1053.
(45) de Groot, F.; Kotani, A. *Core Level Spectroscopy of Solid*; Taylor & Francis: London, 2008.
(46) Neese, F.; Solomon, E. I. *Inorg. Chem.* **1999**, *38*, 1847.

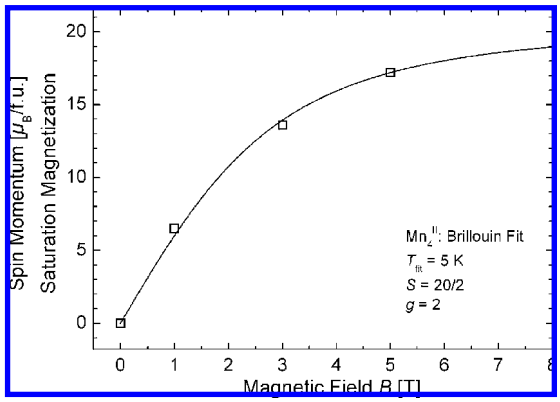

Figure 9. Experimental data of the spin magnetic moment determined at external fields of 0, 1, 3, and 5 T (squares) and the fit of the magnetization by the Brillouin function (solid line). We fitted the magnetization curve by means of a Brillouin function.

Table 6. Spin and Orbital Moments As Obtained from the Experimental XMCD Data at External Magnetic Field Strength

1 T	3 T	5 T
m_{spin} = 6.51 μ_B/fu	m_{spin} = 13.62 μ_B/fu	m_{spin} = 17.15 μ_B/fu
m_{orb} = 0.10 μ_B/fu	m_{orb} = 0.17 μ_B/fu	m_{orb} = 0.36 μ_B/fu

function considering a simple ionic state for the Mn^{2+} ions and a sample temperature of 5 K during the XMCD experiments. Thus, this result is also a nice manifestation of the weak coupling constants between the central ion and the three outer ions, leading to an overall weak ferromagnetic coupling in quite moderate external magnetic fields. See also sections 3.3 and 3.4 (magnetic measurements and ab initio theory).

3.5. Electronic Structure Calculations of the $Mn^{II}_4O_6$ Core. In setting up our calculations, we allowed different orientations of the spin moments at manganese atoms; all magnetic solutions turned out to be stable, with nearly identical values of local magnetic moments and charges (according to the Mulliken population analysis). Moreover, the local densities of states (LDOSs) calculated for different magnetic configurations are almost indistinguishable. This reveals a high enough localization of the electronic states that are responsible for magnetic behavior (mostly Mn 3d, with a slight admixture of O or N 2p) on manganese centers. Obviously, there is a difference in LDOSs at the central and peripheral manganese atoms, which are in different chemical environments. Moreover, among the peripheral manganese atoms, which are structurally (topologically) identical, one differs from two others because of the specific packing of molecular units in the crystal and a slight difference in the bond lengths resulting from that. This means that each star-shaped molecule does not quite have a 3-fold symmetry axis but rather a variation of a mirror-plane symmetry. Correspondingly, for the sake of fitting the results to the Heisenberg (or any other) model, one should allow two distinct center−peripheric (strong) couplings and, in principle, two peripheric−peripheric (weak) ones.

Table 7 gives the data for the total (overall orbitals) Mulliken occupation numbers and HOMO−LUMO energies in both spin channels, for all magnetic configurations considered, in the nominal (experimental determined) structure. The total energies are also given, relative to the lowest one (that for the situation with the central spin opposite to three others). The configurations are numbered by combinations of U and D letters, according to up or down spin setting on four manganese atoms 1, 2, 3, and 1* (see Figure 10). We consider only eight nonequivalent configurations; the other eight can be obtained by inverting the spins on all atoms.

Table 7. Local Magnetic Moments (in μ_B) on Manganese Atoms (1, 2, 3, and 1*), Total Magnetic Moment per Molecule M, HOMO−LUMO Energy Difference, and Total Energies (Relative to the Ground-State Configuration) for Different Magnetic Configurations of the "Manganese-Star" Molecule

config	1	2	3	1*	M (μ_B)	HOMO−LUMO (eV)	ΔE_{tot} (meV)
UUUU	4.68	4.71	4.69	4.68	20	0.404	12.20
DUUU	−4.68	4.70	4.69	4.68	10	0.439	7.38
UDUU	4.68	−4.70	4.69	4.68	10	0.523	0.00
UUDU	4.68	4.70	−4.69	4.68	10	0.424	8.90
UUUD	4.68	4.70	4.69	−4.68	10	0.440	7.33
DDUU	−4.68	−4.70	4.69	4.68	0	0.453	4.36
DUDU	−4.68	4.70	−4.69	4.68	0	0.459	4.42
DUUD	−4.68	4.70	4.69	−4.68	0	0.519	2.64

The fact that the local magnetic moments are almost insensitive to the orientation is an argument in favor of the validity of the Heisenberg model, even if a priori we cannot be sure that the correction terms to it are not important. As a spin value to use in the Heisenberg fit, we took the nominal value $S = {}^5/_2$ because this is exactly a change by 10 μ_B/molecule accompanying an inversion of a single manganese spin. All magnetic configurations studied have a pronounced band gap and are therefore easily identifiable as corresponding to an inversion of $S = {}^5/_2$ spins. The difference from the nominal number ($m_{Mn} \sim 4\ \mu_B$), following from the Mulliken populations, merely indicated that this "rigid" moment is not fully localized at the manganese site but involves some admixture from the ligand states. For the $S = {}^5/_2$ spin, one can be relatively sure about the unimportance of orbital moment and anisotropic exchange terms, even if this would, in principle, need to be checked.

The least-squares fit to the Heisenberg Hamiltonan (eq 1) with four Heisenberg exchange parameters as marked in the right panel of Figure 10, from seven energy differences of Table 7 yields the following values: $J = -2.26$ K, $J' = -1.38$ K, $J_1 = -0.08$ K, and $J'_1 = -0.03$ K (−1.57, −0.96, −0.06, and −0.02 cm^{-1}, respectively). Whereas all interaction parameters are antiferromagnetic, the J_1 and J'_1, which account for "second-neighbor" manganese interaction, are, in fact, negligible. Of the remaining two, the J that couples the central manganese to its nearest peripheric counterpart is dominant.

Comparing these results with the above parameters from the magnetization fit (+0.32 and −0.2 cm^{-1} for J and J',

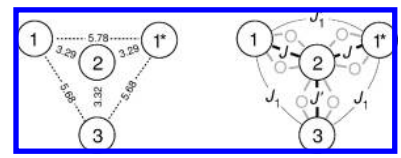

Figure 10. Left panel: distances (in Å) between manganese atoms in the "manganese star" molecule. Right panel: labeling of corresponding different exchange parameters.

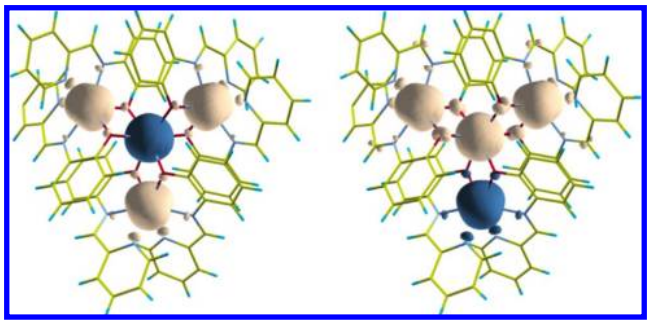

Figure 11. Isosurfaces of spin density corresponding to ±0.05 e/Å^3 for UDUU (left panel) and UUDU (right panel) configurations. Positive and negative magnetic density is shown by two colors.

respectively), one marks opposite signs of the dominant interaction, as they follow from the experiment and theory. This is unusual because typically the DFT (in whatever practical scheme) is accurate enough to yield not only the sign but also the order of magnitude of exchange parameters, overestimating their value, however, by a factor of 3−5 (due to an underestimation of correlation effects within strongly localized d shells). This "consistency" in the order of magnitude between experiment and theory holds also in the present case: the interaction parameters calculated for the "manganese star" molecule are by a factor of ∼50 smaller than those estimated for the "ferric star",[11,12] a $Fe^{III}[Fe^{III}L_2]_3$ star-type molecule with similar 3d ion topology and bridging as the present one but different types of ligands L.

The experimental situation (J positive and of larger absolute value than the negative J') would favor, among the configurations listed in Table 7, the UUDU one. According to the DFT, this configuration is almost degenerate with the other two, in which one or another of the peripheric spins is set antiparallel to three others, ferromagnetically coupled. The energy separation from the DFT ground state (with the central spin inverted) is merely ∼8 meV. A possible explanation of the experiment vs DFT controversy could be that strong interaction of DUUU, UUDU, and UUUD states yields a mixed ground state, whose energy is lower than that of the pure UDUU state.

Figure 11 shows spin-density isosurfaces in the UDUU (nominal DFT ground state) and UUDU (its apparent competitor, according to experiment) configurations. The spin-density level is chosen in the figure to be very low in order to show the spilling of magnetic density from manganese over neighboring oxygen and nitrogen atoms. Isosurfaces for a slightly higher spin-density level would have been nearly spherical, centered at the manganese atoms. One sees that the spilling of the local magnetic moment from manganese onto its nitrogen neighbors is not affected by the magnetic configuration. This visual impression from Figure 11 is confirmed by the Mulliken population analysis for nitrogen magnetic moments, which are on the order of 0.015−0.030 μ_B and stable (changing from one configuration to the other) within 20%. The Mn(2)−Mn(3) bridging oxygens also maintain their induced local moment (of ∼0.02 μ_B, parallel to that of the peripheric manganese). On the contrary, the magetic moments induced on Mn(1)−Mn(2) oxygen bridge atoms within the "ferromagnetic" Mn(1)−Mn(2)−Mn(1*) fragment of UUDU are 2 times larger (∼0.04 μ_B) than those in the corresponding "ferrimagnetic" block of the UDUU configuration. An intriguing question arises of whether this apparently different magnetization of bridge oxygen atoms could ever be probed by experimental techniques. The "differently itinerant" character of the magnetic density in two compared configurations, UDUU vs UUDU, may also play a role in determining their relative stability. An argumentation here may be that the DFT generally underestimates the tendency toward charge localization in similar systems; therefore, the level of the "DFT error" can be different in slightly more localized and slightly less localized situations. This can be important here, in view of very small energy differences between competing configurations.

Another point to consider, in view of rather small values of exchange parameters J, is their possible dependence on the details of the crystal structure, in both experiment and theory. In order to further analyze a competition between UDUU and UUDU configurations, we allowed independent structural relaxation in these two magnetic states. This led to an overall energy lowering by ∼30 eV/molecule, maintaining, however, the energy difference between two separately relaxed cases within 15 meV. On the average, we found good agreement with experimentally measured structures: the "long" Mn(1,1*)−Mn(2) distances are 3.285 Å (UUDU-relaxed) and 3.281 Å (UDUU-relaxed), to be compared to the measured 3.286 Å; the "short" Mn(3)−Mn(2) distances are 3.351, 3.350 and 3.322 Å, correspondingly, and the Mn−O−Mn angles (≈99° for the short bridges and ≈101° for the long bridges) agree within 1.5° throughout the three structures. Still, the minute structural differences produce markedly different exchange constants: $J \sim -0.6$ K and $J' \sim -0.1$ K, as estimated from the energy differences (similar to those in Table 7) in the UUDU-relaxed structure.

The obtained "scattering" of calculation data ($J \sim -2.2/-0.6$ K) can serve to estimate the "empirical" accuracy of the DFT treatment in our case, in addition to possible basic limitations of DFT, in the extraction of exchange interaction parameters. Our results show that, because magnetic interactions in the manganese star are quite weak, small variations of the crystal structure with temperature or in the magnetic field may have a non-negligible effect on the *definition* and *extraction* of the J parameters.

The LDOS (Figures 12 and 13) and spin density plots (Figure 11) discussed in the following are as obtained for the nominal DFT ground state (UDUU configuration).

Both figures reveal a fair amount of localization of the Mn 3d states, with weak but appreciable admixture to O 2p and N 2p states (that is responsible for binding the manganese atoms into a molecule). LDOS at two manganese sites have similarities, but the differences cannot be overlooked. The splitting into t_{2g} and e_g bands, particularly pronounced in the region of vacant states, is more net for (the central) Mn(2), which is in a more perfect octahedral environment, whereas that around Mn(1) is considerably distorted.

Figure 12 displays the calculated partial densities of states (pDOS) of Mn 3d, O 1s, and N 1s. These states are largely

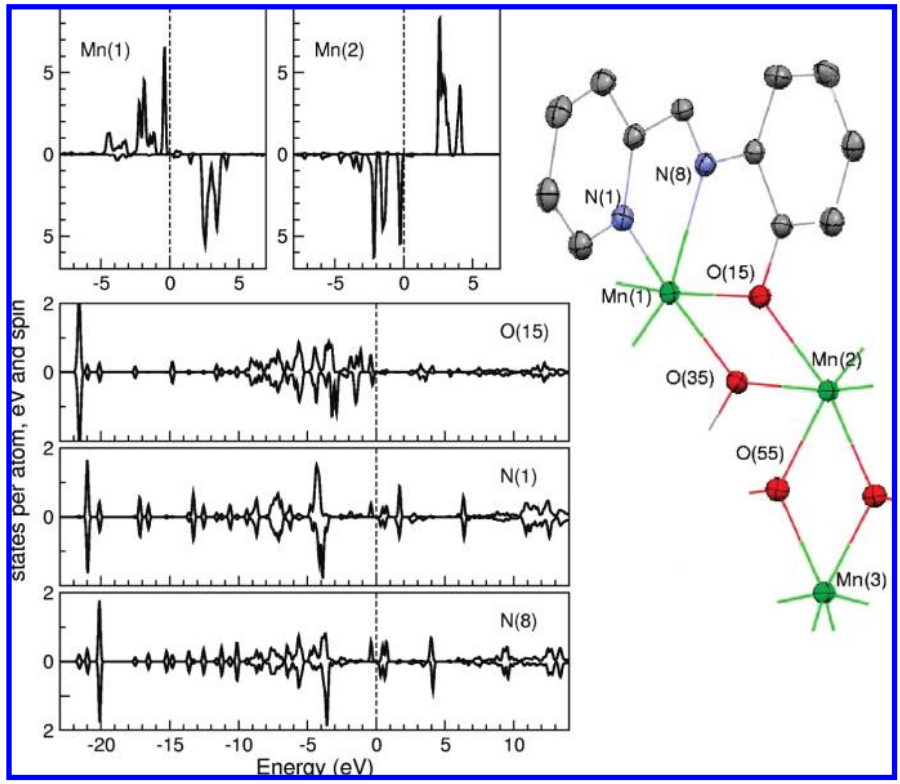

Figure 12. LDOSs of two manganese atoms and their 2p-type neighbors, calculated for the "manganese star" molecule in magnetic ground-state configuration UDUU. The numbering of atoms is shown in the inset.

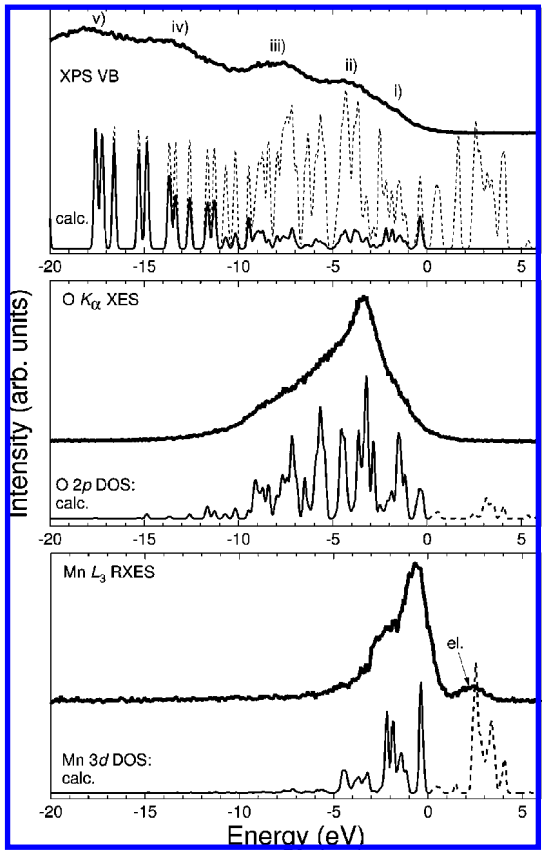

Figure 13. XPS valence band region (tDOS) compared to corresponding DFT calculations. The photoionization cross sections were taken into account for the solid line. Lower panels: XES spectra of the Mn L edge and O K edge in comparison with the calculated pDOSs.

energetically overlapping and form a common valence band going down to ∼−20 eV below the Fermi level. The calculated densities of states can be used to understand the XPS valence band and the Mn and O K XES results (Figure 13). The XES spectra have been brought to a common energy loss scale with the XPS valence band and the calculated densities of states. Thus, in Figure 13, the XES spectra reflect the element-specific partial densities of states. The XPS valence band comprises five distinct features labeled (i)−(v). A broad shoulder spans the range from the Fermi level to about −4 eV, followed by two local intensity maxima at around −5 and −9 eV. Finally bands (iv) and (v) are located between (−13) and (−16) eV and between (−18) and (−22) eV, respectively. With the help of the XES and the calculated pDOS, we can assign band (i) to Mn 3d states, namely, the spin-up states of the outer manganese ions and the spin-down states of the central manganese ion (see the top panel of Figure 12). Feature (ii) comprises also a considerable amount of Mn 3d states, which are likely hybridized with N 2p and O 2p states via charge transfer. However, the relatively weak overlap between the Mn L and O K XES indicates that charge-transfer effects are relatively weak in this compound. Finally, bands (iv) and (v) can be attributed to overlapping of O 2p and C 2s states and to N 2s states, respectively. This is in agreement with other observations pointing toward a weak covalency in the Mn−O bonds: the peaks in the Mn-DOS (of the central atom) are quite narrow and sparse, in contrast to more extended t_{2g}- and e_g-like subbands visible in the density of state of the central atom in the iron star.[12] Moreover, much smaller values of (super)exchange param-

eters in the manganese star, as compared to the iron star, also reveal a lower covalency in the former system.

4. Conclusions

We have studied an $S_t = 10$ high-spin molecule, namely, a star-shaped molecule with the $Mn^{II}_4O_6$ core, leading to a number of interesting results. A detailed X-ray structural analysis has been performed. Magnetic susceptibility measurements exhibit weak exchange coupling constants between the four Mn^{2+} ions. Thus, the magnetization measurements indicate complicated low-lying states in which the ground state is not well-separated, resulting from a dominant weak ferromagnetic coupling and a giant moment of up to 20 μ_B/fu. XMCD measurements reveal that almost the complete magnetic moment is located around the Mn^{2+} ions. Furthermore, we can conclude that a few charge-transfer states are present; charge-transfer multiplet calculations reveal 93.8% $3d^5$ and 6.2% $3d^6\underline{L}$ configurations. Finally, electronic structure calculations confirm that the interaction parameters are much smaller (by a factor of ~50) than those for related compounds like the "ferric star" molecule.[12] The "manganese star" is a very interesting prototype for polymetallic complexes with weak exchange coupling constants.

Acknowledgment. E. Arenholz and J. D. Denlinger are acknowledged for excellent technical support. We thank J. Schnack and M. Brüger for helpful discussions. Financial support by the Graduate College 695, Deutsche Forschungsgemeinschaft (Priority Program "Molecular Magnetism"), and the Ph.D. program (Lower Saxony) is gratefully acknowledged. Part of the work was performed at the ALS, which is supported by the U.S. Department of Energy under Contract DE-AC03-76SF00098.

IC7023007